

Detectability of non-differentiable generalized synchrony

Nikolai F. Rulkov¹ and Valentin S. Afraimovich²

¹*Institute for Nonlinear Science, University of California, San Diego, La Jolla, CA 92093-0402*

²*IICO-UASLP, A. Obregón 64, 78000 San Luis Potosí, SLP, México*

Generalized synchronization of chaos is a type of cooperative behavior in directionally-coupled oscillators that is characterized by existence of stable and persistent functional dependence of response trajectories from the chaotic trajectory of driving oscillator. In many practical cases this function is non-differentiable and has a very complex shape. The generalized synchrony in such cases seems to be undetectable, and only the cases, in which a differentiable synchronization function exists, are considered to make sense in practice. We show that this viewpoint is not always correct and the non-differentiable generalized synchrony can be revealed in many practical cases. Conditions for detection of generalized synchrony are derived analytically, and illustrated numerically with a simple example of non-differentiable generalized synchronization.

PACS numbers: PACS number(s): 05.45.Xt

I. INTRODUCTION

Synchronization plays an important role both for understanding of cooperative behavior in natural networks of oscillators [1] and for various engineering applications [2, 3]. Recently a significant interest in understanding and theoretical description of synchronization regimes among the oscillators with chaotic behavior is perceived, see for example recent books and reviews [4, 5, 6]. Various types of chaos synchrony, whose description may require different theoretical frameworks, were found in natural systems and specified. These types of synchrony include identical synchronization [7, 8, 9], generalized synchronization [10, 11, 12, 13] and phase synchronization [14, 15].

The framework of generalized synchronization was proposed as an attempt to extend the classical theory of forced synchronization of a periodic oscillator, initiated by the works of van der Pol [16], Andronov and Witt [17], to the case of directionally coupled chaotic oscillators. This framework defines synchronization as the onset of conditional stability of a chaotically driven oscillator, and as the existence of a functional relation that maps the chaotic trajectory of driving oscillator into the trajectory of driven oscillator [10, 18]. In the case of invertible dynamics of driving system such functional relation is usually substituted with a function that maps the state of driving system into the state of response one when these states are measured simultaneously. Rigorous mathematical results indicate that, depending on the strength of conditional stability, the synchronization function can be differentiable or non-differentiable [19, 20, 21, 22, 23]. In many experimental studies researcher needs to establish the fact of chaos synchronization when direct analysis of conditional stability is hardly possible. In such a situation the detection of generalized chaos synchrony characterized by a non-differentiable function, which due to dense wrinkles, cusps and finite number of points appears as a thick and fuzzy set, may seem to be impossible [20, 24, 25].

In this paper we show that detectability of the non-differentiable synchrony can be significantly improved and become feasible if one explores synchronization function taking into account additional points on sufficiently long intervals of the driving trajectory preceding to the current state. The paper is organized as follows. In Section II we discuss the idea of such detectability and evaluate the improvement using numerical analysis of a simple example. Section III develops a theoretical arguments explaining the mechanism behind the detectability improvement. Section IV discusses possible effects caused by small additive noise in the data. Summary of the results and possible applications are discussed in the Conclusion.

II. NUMERICAL EXAMPLE

To illustrate the idea of detectability enhancement we first consider an example of a drive-response system which was proposed and studied in [20]. In this example generalized baker map

$$x_{n+1}^{(1)} = \begin{cases} \lambda_a x_n^{(1)}, & \text{if } x_n^{(2)} < a, \\ \lambda_a + \lambda_b x_n^{(1)}, & \text{if } x_n^{(2)} \geq a, \end{cases} \quad (1a)$$

$$x_{n+1}^{(2)} = \begin{cases} x_n^{(2)}/a, & \text{if } x_n^{(2)} < a, \\ (x_n^{(2)} - a)/b, & \text{if } x_n^{(2)} \geq a, \end{cases} \quad (1b)$$

where $0 \leq x_n^{(i)} < 1$, $\lambda_a = 1 - \lambda_b = 0.3$, and $a = 1 - b = 0.5$, drives a system of the form

$$y_{n+1} = cy_n + \cos(2\pi x_n^{(1)}). \quad (2)$$

Here parameter c defines the properties of the response behavior. Consider the systems dynamics within the parameter interval $0 < c < 1$. In this case response system (2) is conditionally stable. The dynamics of driving system (1) is invertible and according to the theory (see, for example [22, 23]) there exists a continuous function

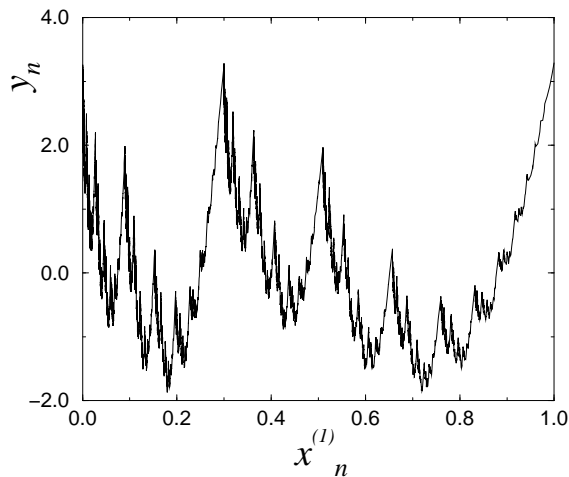


FIG. 1: The shape of the function $y_n = h(x_n^{(1)})$ computed with $c = 0.7$.

$y_n = h(\mathbf{x}_n)$, where $\mathbf{x}_n = (x_n^{(1)}, x_n^{(2)})$. Due to the specific form of the driving and response systems function h , in our case, is independent of $x_n^{(2)}$. Indeed, given the value of $x_n^{(1)}$ all previous values of this variable can be found from equation (1a), when one iterates this one-dimensional map backward in time, and these values are independent of $x_n^{(2)}$. Therefore, function h can be plotted as a graph in the variables plane $(x_n^{(1)}, y_n)$.

The example of non-differentiable function h computed with $c = 0.7$ is shown in Fig. 1. It is clear from the shape of the function that, in practical situation with a similar function, the existence of the function cannot be revealed from such a plot because the states of response system measured for nearby states of driving system can be very disperse. This situation can make one to believe that the onset of non-differentiable generalized synchronization is practically undetectable. The statements on such practical undetectability are usually made when one analyses only relation between simultaneous states in the attractors of driving and response systems. One may ask a question if additional information about the chaotic trajectory can help to resolve the complexity of this functional relation? And if the answer is yes, what properties of the non-differentiable function can be improved?

To illustrate positive answer to the first question we adopt the approach developed in [26] and consider the additional information about the driving chaotic trajectory \mathbf{x}_n using its symbolic description. Now we define the state of the driving system as the value of $x_{n-m}^{(1)}$ and the symbolic sequence $[\alpha_1, \dots, \alpha_m]$ generated in the next consecutive iterations towards $x_n^{(1)}$. In the considered example symbols α_i can be easily defined from the evolution of variable $x_n^{(2)}$. If $x_{n-i}^{(2)} < a$, then $\alpha_i = 0$. If $x_{n-i}^{(2)} \geq a$, then $\alpha_i = 1$. From the data generated by the maps (1), (2) we can examine synchronization func-

tion in a new form $h^{(m)}$ which is defined as a mapping $([\alpha_1, \dots, \alpha_m], x_{n-m}^{(1)}) \rightarrow y_n$.

In order to illustrate the improvement of the modified synchronization function $h^{(m)}$ with the increase of m we plot y_n versus $([\alpha_1, \dots, \alpha_m], x_{n-m}^{(1)})$ for two fixed symbolic sequences that differ by two most recent symbols. The cases of $m = 4$ and $m = 8$ are presented in Fig. 2a and b respectively, where the parameters of the maps are the same as in Fig. 1. Comparing these plots with the plot shown in Fig. 1 one can see that the existence of synchronization function becomes more apparent as the delay m increases. Notice, that the scales of corresponding axes in these plots are the same.

We studied how the complex image of synchronized attractors in the space of a drive-response system converges to a "good" simple function with the increase of m . We analyzed the sets of attractor points conditioned by all possible symbolic masks α of various lengths m . For each mask of preceding symbols $S_m^i = [\alpha_1, \dots, \alpha_m]$ we computed the best polynomial fitting function $\phi_{S_m^i}(x)$ of order 30 using Singular Value Decomposition (SVD) algorithm, and studied the dependence of mean squared error (E_{MS}), averaged over all masks of length m , on the value of m . This dependence computed for four different values of c is shown in Fig. 3.

One can see from Fig. 3 that E_{MS} decreases exponentially fast when m increases. Approximating this dependence with exponential,

$$E_{MS}(m) \sim e^{\Lambda m}, \quad (3)$$

one can find the rate of convergence Λ . Figure 4 shows how the convergence rate Λ evolves with the change of parameter value c . The absolute value of Λ decreases as the value of c grows. This indicates that for higher values of c the synchronization function becomes more complex [20] and its detection with a given resolution requires more information on the driving trajectory than for lower values of c .

One can easily check that when $c \rightarrow 1$, the conditional dynamics of response system (2) approaches the threshold of instability and, as the result, synchronization terminates and function h disappears. The plot of Λ vs c reflects this fact and one can see from Fig. 4 that convergence rate Λ tends to zero as $c \rightarrow 1$. It can be shown that the linear dependence of Λ on $\log(c)$ is due to the fact that the response system in this example is a linear system and $\log(|c|)$ is the contraction rate of its phase volume.

To get a better view on the function improvement, examine how additional symbolic information collected along the driving trajectory changes the shape of the whole synchronization function. One way of taking such symbolic information into account is to compute the integer value out of binary symbolic mask S_m^i and, then, supplement this integer with the fractional value given by $x_{n-m}^{(1)}$. Note that in our case $0 \leq x_{n-m}^{(1)} < 1$. Computing the integer part we assume that the most recent symbol

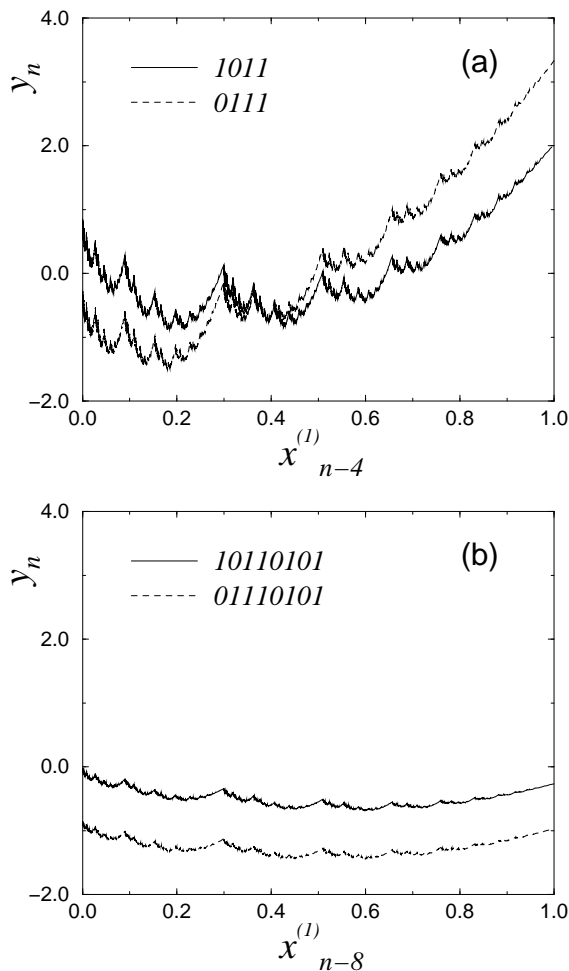


FIG. 2: The synchronization function computed using additional symbolic information on the driving trajectory for the case shown in Fig 1. Only two symbolic masks of each length m are presented. The case $m = 4$ is shown in panel (a) and $m = 8$ is in panel (b).

α_1 of mask S_m^i is the most significant bit. As the result we obtain the decimal values of the form $I(S_m^i) \cdot x_{n-m}^{(1)}$. Every decimal value is considered as a new argument of the modified synchronization function $h^{(m)}$. Figure 5 presents such a function plotted for three different values of m . One can see that for large m ($m > 4$), the overall shape and complexity of the function remains about the same, but the interval of the argument increases in size by factor 2^m . This indicates that there exists some kind of self-similarity of the non-differentiable synchronization function, and the enhanced detectability is the result of more precise evaluation of the state of the driving system. It is important to note that the precision of the state evaluation increases with m despite the fact the values of variable $x^{(1)}$ are measured with the same precision as before.

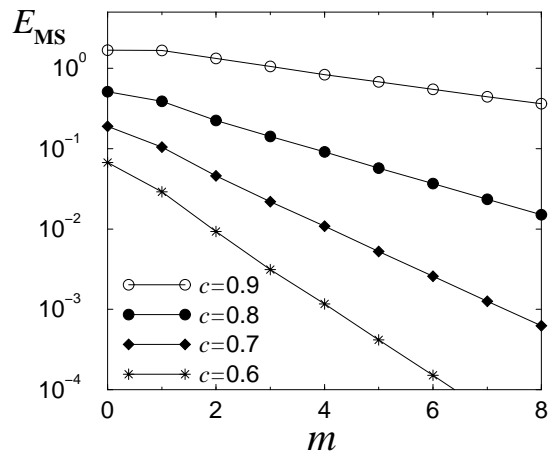


FIG. 3: The dependence of mean squared error of best polynomial fitting function for the attractor points (x_{n-m}, y_n) on the length m of the preceding masks S_m^i .

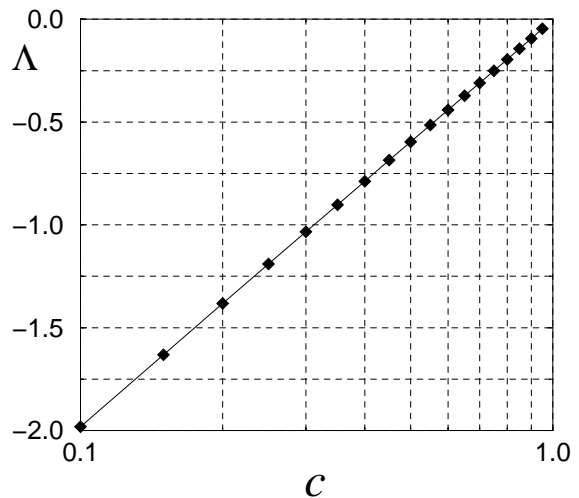


FIG. 4: The dependence of convergence rate Λ on the value of coupling parameter c plotted in the logarithmic scale.

III. THEORETICAL RESULTS

The example considered above clearly indicates that the functional relation between the synchronized system becomes more apparent when length of driving trajectory taken for the analysis increases. In order to examine which properties of the non-differentiable function change and simplify the detection of the functional relation we present the following theoretical analysis.

In this section we shall concentrate on systems with a unidirectional coupling (or systems with a skew product

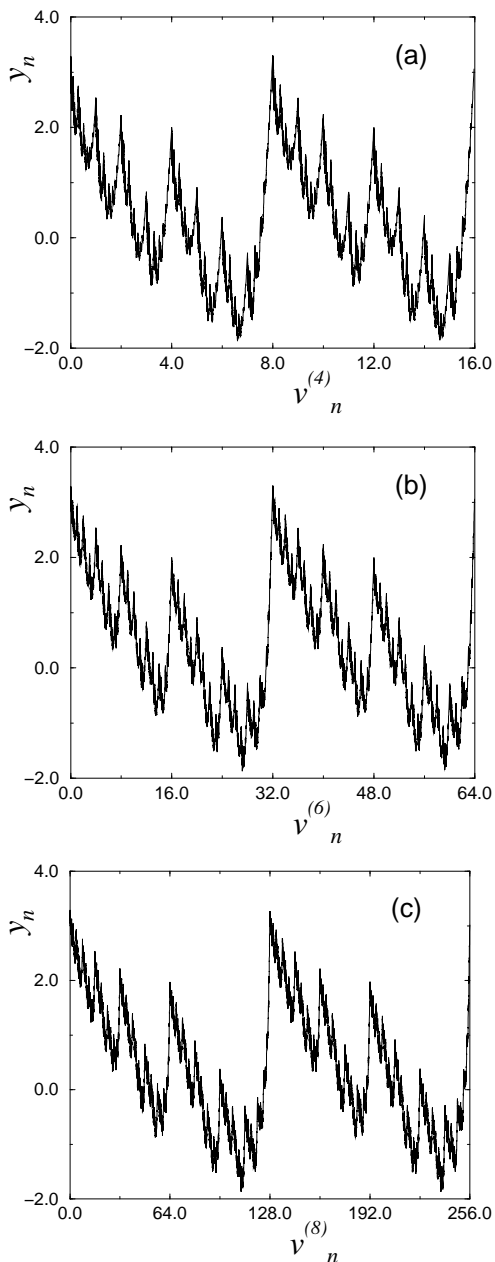


FIG. 5: The synchronization function shown in Fig. 1 plotted versus a new variable $v_n^{(m)} := I(S_m^i).x_{n-m}^{(1)}$ that contains symbolic information about the driving trajectory. Panel (a) shows the case $m = 4$, (b) $m = 6$, and (c) $m = 8$. Note the changes in the values of the horizontal axes.

structure) of the form:

$$\begin{aligned} x' &= f(x) \\ y' &= g_\rho(x, y). \end{aligned} \quad (4)$$

These equations determine a map $F_\rho : (x, y) \mapsto (x', y')$ generating a dynamical system. The first subsystem is called the driving system, the second subsystem is called the response system and ρ is a parameter that controls

the coupling strength. The fact of synchronization in this systems means that there is a region of parameter values ρ in which, for any initial conditions (x_0, y_0) , (x_0, \tilde{y}_0) ,

$$\lim_{n \rightarrow \infty} \text{dist}(y_n, \tilde{y}_n) = 0, \quad (5)$$

where $(x_n, y_n) = F_\rho^n(x_0, y_0)$ ($(x_n, \tilde{y}_n) = F_\rho^n(x_0, \tilde{y}_0)$). Loosely speaking, this means that, for any initial conditions, the distance between the states of the slave subsystem goes to zero with time.

We assume for the sake of definiteness, that in the system (4) one has $x \in \mathbb{R}^d$ and $y \in \mathbb{R}^\ell$, and that g_ρ is continuous and f is a homeomorphism. Since we study dissipative systems we also assume that there exists a ball of dissipation $B \subset \mathbb{R}^{d+\ell}$, i.e. $F_\rho(B) \subset \text{Int}(B)$ for any $\rho \in S$, where S is a region in ρ -space (in which the system (4) exhibits synchronization). Without loss of generality we assume that $B = B_x \times B_y$, i.e. B is a rectangle, where B_x (resp. B_y) is a ball in x -space (resp. y -space). Denote by \mathcal{A}_ρ the maximal attractor in B , i.e. $\mathcal{A}_\rho = \bigcap_{n=0}^{\infty} F_\rho^n(B)$.

Through this section we shall assume that one-to-one globally stable generalized synchronization occurs in B , i.e. the condition (5) satisfy when (x_0, y_0) and (x_0, \tilde{y}_0) are arbitrary points in B .

It was shown in [23] that under these conditions there is a continuous functional dependence between x and y -components of orbits while the system is in synchronized region. To obtain more detailed characteristics about this functional dependence we need an additional assumption. Assume that

$$|y_{n+1} - \tilde{y}_{n+1}| \leq c|y_n - \tilde{y}_n| \quad (6)$$

where $c < 1$. Of course the parameter c is a function of ρ . For the sake of simplicity, we assume that $c = \rho$. Thus,

$$|y_{n+1} - \tilde{y}_{n+1}| \leq \rho|y_n - \tilde{y}_n|, \quad 0 < \rho < 1. \quad (7)$$

It follows that

$$|g_\rho(x, y) - g_\rho(x, \tilde{y})| \leq \rho|y - \tilde{y}| \quad (8)$$

for any $(x, y), (x, \tilde{y}) \in B$. Let us draw the attention on the fact that the smaller ρ is, the greater the coupling strength.

Assumption (7) implies that $|y_n - \tilde{y}_n|$ goes to zero exponentially fast, and this fact allows one to prove that function $h : x_n \mapsto y_n$ is Hölder continuous provided that the functions f and g_ρ have good smooth properties, or at least they are Lipschitz-continuous. So we assume that:

$$|f(x) - f(\tilde{x})| \leq \gamma_+|x - \tilde{x}| \quad (9)$$

and

$$|f^{-1}(x) - f^{-1}(\tilde{x})| \leq \gamma_-|x - \tilde{x}|, \quad (10)$$

where $\gamma_-, \gamma_+ \geq 1$. Here γ_+ characterizes the rate of divergence of nearby driving trajectories forward in time,

and γ_- characterizes their divergence backward in time. Moreover, we assume that:

$$|g_\rho(x, y) - g_\rho(\tilde{x}, y)| \leq \eta|x - \tilde{x}| \quad (11)$$

for any $(x, y), (\tilde{x}, y) \in B$, where $\eta > 0$.

The following statement was proved in [23].

Theorem 1 (Hölder property) *Under assumptions (8)-(11) the function h is Hölder continuous, i.e. for any $0 < \alpha < \alpha_0$, $x, \tilde{x} \in \mathcal{A}_{\rho, x}$ one has:*

$$|h(x) - h(\tilde{x})| \leq 2a|x - \tilde{x}|^\alpha \quad (12)$$

where

$$\alpha \leq \alpha_0 \equiv \left(1 - \frac{\log(\gamma_+ \gamma_-)}{\log \rho}\right)^{-1}, \quad (13)$$

and $a \geq a_0$, where $a = a_0$ is the solution of the equation:

$$a = \frac{\eta}{\gamma_+ - \rho} a^{\frac{\log(\gamma_+ \gamma_-)}{\log \rho}} (\gamma_+ \gamma_-)^{1 - \frac{\log |B_y|}{\log \rho}}.$$

Here $|B_y|$ stands for the diameter of B_y . Recall that Hölder exponents quantify the “degree of non-differentiability”.

Our goal is to understand what happens if one tries to study the dependence between the y -coordinate of the orbit at iteration n and the x -coordinate at the moment $n - m$, for $m > 0$. In other words we are going to study the effect of the “delay” onto the functional dependence in the synchronized region. The following result holds:

Theorem 2 *Let conditions of Theorem 1 be satisfied and $(x_n, y_n), (x'_n, y'_n)$ be orbits belonging to \mathcal{A}_ρ . Then for every $\epsilon > 0$ there exists $\delta > 0$ such that for every pair x_{n-m}, \tilde{x}_{n-m} , $|x_{n-m} - \tilde{x}_{n-m}| < \delta$ one has*

$$|y_n - \tilde{y}_n| \leq A|x_{n-m} - \tilde{x}_{n-m}|^\alpha \quad (14)$$

where

$$\alpha \leq \alpha_0 + \beta(\epsilon), \quad \alpha_0 \equiv \left(1 - \frac{\log(\gamma_+ \gamma_-)}{\log \rho}\right)^{-1}, \quad (15)$$

and $A \geq A_m$, where

$$A_m = \epsilon + \varrho \gamma_-^{-m} \quad (16)$$

and ϱ is a constant independent of m .

Proof. Without loss of generality we prove the estimate (14) for $n = 0$. The proof for another values of n is the same. Let $\mathcal{A}_{\rho, x} \equiv \Pi_x \mathcal{A}_\rho$ be the image of \mathcal{A}_ρ under the natural projection Π_x to \mathbb{R}^d .

Consider a point $x_0 \in \mathcal{A}_{\rho, x}$. Let $x_{-i} \equiv f^{-i}(x_0)$. Given the backward orbit $\{x_{-i}\}_{i=0}^\infty$, the dynamics on B_y is defined by the sequence of operators $\{g_\rho(x_{-i}, \cdot)\}_{i=0}^\infty$ acting on B_y . Define the following operation:

$$(g_\rho \star g_\rho)(x, y) \equiv g_\rho(f(x), g_\rho(x, y)).$$

We denote by $g_\rho^{\star k}(x, y)$ the result of the operation ‘ \star ’ performed k times (by convention $g_\rho^{\star 0} \equiv g_\rho$). Notice that $g_\rho^{\star k}(x, y) = \Pi_y F_\rho^k(x, y)$.

Consider two points (x_0, y_0) and $(\tilde{x}_0, \tilde{y}_0)$ in the attractor, i.e. $y_0 = h(x_0)$, $\tilde{y}_0 = h(\tilde{x}_0)$. Their backward orbits up to time k are also contained in the attractor. We denote them by:

$$(x_{-k}, y_{-k}), \dots, (x_{-1}, y_{-1}), (x_0, y_0)$$

and

$$(\tilde{x}_{-k}, \tilde{y}_{-k}), \dots, (\tilde{x}_{-1}, \tilde{y}_{-1}), (\tilde{x}_0, \tilde{y}_0).$$

By construction we have that:

$$\begin{aligned} x_0 &= f^k(x_{-k}) \\ y_0 &= g_\rho^{\star k}(x_{-k}, y_{-k}) \end{aligned}$$

and

$$\begin{aligned} \tilde{x}_0 &= f^k(\tilde{x}_{-k}) \\ \tilde{y}_0 &= g_\rho^{\star k}(\tilde{x}_{-k}, \tilde{y}_{-k}). \end{aligned}$$

From these equations we can estimate $|y_0 - \tilde{y}_0|$. Indeed, triangle inequality yields:

$$|y_0 - \tilde{y}_0| \leq |g_\rho^{\star k}(x_{-k}, y_{-k}) - g_\rho^{\star k}(x_{-k}, \tilde{y}_{-k})| + |g_\rho^{\star k}(x_{-k}, \tilde{y}_{-k}) - g_\rho^{\star k}(\tilde{x}_{-k}, \tilde{y}_{-k})| \quad (17)$$

The first term on the right can be bounded using the contracting property of g :

$$|g_\rho^{\star k}(x_{-k}, y_{-k}) - g_\rho^{\star k}(x_{-k}, \tilde{y}_{-k})| \leq \rho^k |B_y|, \quad (18)$$

where $|B_y|$ stands for $\text{diam}(B_y)$. The second term can be bounded by:

$$|g_\rho^{\star k}(x_{-k}, \tilde{y}_{-k}) - g_\rho^{\star k}(\tilde{x}_{-k}, \tilde{y}_{-k})| \leq L_k |x_{-k} - \tilde{x}_{-k}|, \quad (19)$$

where L_k is the Lipschitz constant of $g_\rho^{\star k}(\cdot, y)$. According to Lemma 16 in the paper [23]

$$L_k \leq \frac{\eta}{\gamma_+ - \rho} \gamma_+^k. \quad (20)$$

Using assumption (10) one gets:

$$|x_{-k} - \tilde{x}_{-k}| \leq \gamma_-^{k-m} |x_{-m} - \tilde{x}_{-m}|. \quad (21)$$

Putting together these inequalities, one obtains for all k :

$$|y_0 - \tilde{y}_0| \leq \rho^k |B_y| + \frac{\eta}{\gamma_+ - \rho} \gamma_-^{-m} (\gamma_+ \gamma_-)^k |x_{-m} - \tilde{x}_{-m}|. \quad (22)$$

Fix an arbitrarily small $\sigma > 0$ and rewrite the first term in (22) as follows

$$\rho^k |B_y| = (\rho + \sigma)^k |B_y| \left(\frac{\rho}{\rho + \sigma}\right)^k. \quad (23)$$

then set

$$(\rho + \sigma)^k \cong |x_{-m} - \tilde{x}_{-m}|^\alpha. \quad (24)$$

Therefore using standard logarithmic identity

$$(\gamma_+ \gamma_-)^k \equiv G^{k \log_G(\gamma_+ \gamma_-)}$$

with $G = |x_{-m} - \tilde{x}_{-m}|$, and formula(24) one can write

$$(\gamma_+ \gamma_-)^k \cong |x_{-m} - \tilde{x}_{-m}|^{\frac{\alpha \log(\gamma_+ \gamma_-)}{\log(\rho + \sigma)}} \quad (25)$$

Let $\alpha = \alpha(\sigma) = \left(1 - \frac{\log(\gamma_+ \gamma_-)}{\log(\rho + \sigma)}\right)^{-1}$. Then (22) implies

$$|y_0 - \tilde{y}_0| \leq \left(\left(\frac{\rho}{\rho + \sigma}\right)^k |B_y| + \frac{\eta}{\gamma_+ - \rho} \gamma_-^{-m} \right) \times |x_{-m} - \tilde{x}_{-m}|^{\alpha(\sigma)} \quad (26)$$

Thus, if $|x_{-m} - \tilde{x}_{-m}|$ is small enough then k is large enough because of (24). Therefore, $\left(\frac{\rho}{\rho + \sigma}\right)^k |B_y| < \epsilon$, $\alpha(\sigma) = \alpha_0 + \beta(\epsilon)$, and the statement of Theorem 2 holds. \square

Hence, we have shown that while the Hölder exponent remains the same as for $m = 0$, the Hölder constant A_m given by formula (16) can be as small as we wish provided that points on the graph of the function h are close enough. In the numerical example presented in Sec. II the closeness of driving trajectories was achieved by selecting the trajectories with the same symbolic sequence S_m^i .

IV. EFFECTS OF NOISE

The studies presented in Sections II and III deal with the detectability issues of non-differentiable (wrinkled) synchronization function when data, acquired from drive and response system, are not contaminated by noise. In a realistic situation external noise is always present in the data. Taking into account the complexity of fine structure typical for wrinkled synchronization functions one may expect that even a very small noise in the data ruins the detectability of synchronization. We studied the noise impact using the numerical example considered in Section II. We examined how the convergence of wrinkled function $h^{(m)}$ to a polynomial function is effected by external noise.

The behavior of synchronized systems can be influenced by a noise in many different ways. For example, stochastic forces, applied to response and/or drive system, destroy the functional relation between the systems independently of the complexity of the function shape. The level of destruction in this case will significantly depend upon the dynamical properties of the coupled systems.

To be specific we will examine only the case when the synchronization function exists, but the data representing this function are contaminated with a noise added to

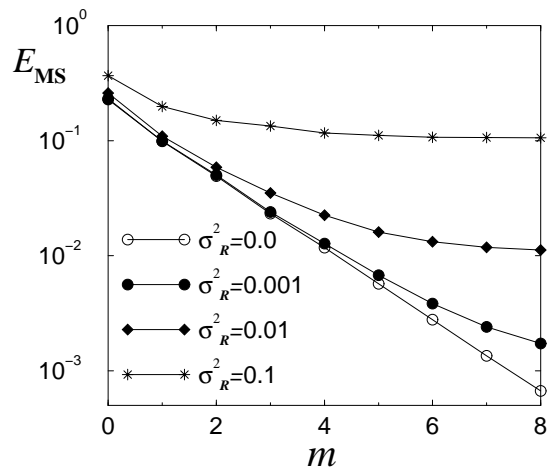


FIG. 6: The dependence of mean squared error of best polynomial fitting function for the attractor points (x_{n-m}, y_n) on the mask length m computed for $c = 0.7$ and four different values of variance σ_R^2 of the noise added to y_n data.

the measurements. Namely, when one deals with the data $x_n^{(1)} + \xi_n$ and $y_n + \zeta_n$, where $x_n^{(1)}$ and y_n are generated by equations (1),(2), and the independent noisy components ξ_n and ζ_n are white Gaussian noise with variances σ_D^2 and σ_R^2 , respectively. In the numerical analysis we will also assume that symbolic sequences of driving trajectory are detected correctly.

We found that ξ_n and ζ_n influence the convergence properties differently. To illustrate it, consider, first, the cases when only one source of noise is present. Figure 6 shows the effect of noise occurred in the measurements of the response system ($\xi_n = 0$ and $\zeta_n \neq 0$) for different values of variance σ_R^2 . Noise of this type sets a limit on the precision of the function resolution, see Fig. 6. The numerical analysis shows that the limit is $E_{MS}^* \approx \sigma_R^2$. This result is quite predictable. Indeed, noise in the response system destroys the function by scattering points along y -variable and makes a thick object (a fuzzy layer) instead of the graph $h^{(m)}$. The thickness of the layer is characterized by the level of noise, namely by σ_R^2 . It is clear that, the size of the thickness (along y - variable) does not change under the transformations applied to the data representing driving trajectory. Since our method is not designed to locate the function inside this fuzzy layer, we cannot expect the accuracy (in terms of E_{RM}) be better than σ_R^2 .

When noise occur in the measurements of driving variable ($\xi_n \neq 0$ and $\zeta_n = 0$) the conversion process has a different dynamics, see Fig. 7. Now the graph of the function in Fig. 1 is transformed into a thick layer due to scattering of data points along variable x . However, as it follows from Fig. 7 that thickness does not limit the precision of function evaluation. This effect can be understood from the considerations presented in Fig. 1 and Fig. 5. Indeed, the increase of trajectory length in the

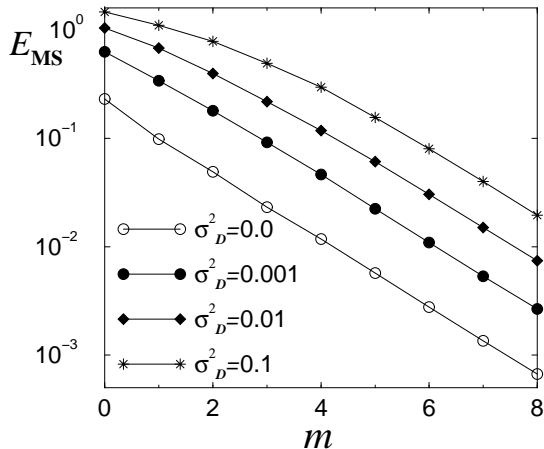


FIG. 7: The dependence of E_{MS} on m computed for $c = 0.7$ and four different values of variance σ_D^2 of the noise added to $x_n^{(1)}$ data.

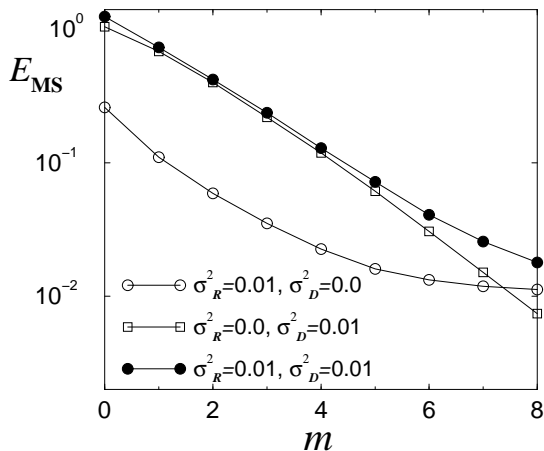


FIG. 8: The dependence of mean squared error of best polynomial fitting function for the attractor points (x_{n-m}, y_n) on the trajectory length m computed for three different n .

analysis of the function is equivalent to rescaling of the function argument, while the overall shape of the function does not change, see Fig. 5. While the interval of the argument values increases with the trajectory length as 2^m the x -size of the thick layer remains unchanged. As the result the increase of m , in this case, improves the precision function detection.

The effects induced by additive noise in the data is summarized in Fig. 8 where the dependence of E_{MS} versus m is shown for three different situation of noise $(\xi_n = 0, \zeta_n \neq 0)$, $(\xi_n \neq 0, \zeta_n = 0)$ and $(\xi_n \neq 0, \zeta_n \neq 0)$. These plots are computed for the coupling strength $c = 0.7$. The results indicate that if the level of noise in the data is small a non-differentiable function is detectable with some accuracy limited by the noise

variance.

In this analysis we assumed that symbolic sequence representing the driving trajectory is detected correctly. We expect that when the symbolic sequence contains errors, then, the function can be severely damaged and, the improvement of function detection can fail. We believe that the use of a noise reduction technique on the data before the computation of E_{MS} versus m plots can be very beneficial in this case.

V. CONCLUSIONS

A simple numerical example and rigorous theoretical analysis show that, despite complex shapes of non-differentiable synchronization functions, the existence of such a function can be detectable in practical situation. This can be achieved by considering this function not as a function of the current state of driving system, but as a function of the state, in which the driving system has been a few steps ago. Thanks to the contracting properties caused the dissipation in the driving system the nearby trajectories disperse far away from each other in the previous times. This effect can be used as a "magnifying glass" in the detection of non-differentiable synchronization function that contains multiple wrinkles and cusps. It is shown that, although the "magnified" function in this analysis remains non-differentiable, the amplitude of these wrinkles and cusps gets smaller as the delay increases.

The results presented in this paper are in agreement with the recent study on detecting of generalized synchrony made by He, Zheng and Stone [27]. Their study based on a different technique that involves the analysis of drive and response trajectories in the embedded phase spaces and takes into account p preimages for each trajectory point. The use of the preimages in this case also acts as a "magnifying glass" in detecting of the wrinkled synchronization function.

In the example considered in Section II, the synchronization function depends only on the $x^{(1)}$ -variable, which is the coordinate that always represents a stable direction in \mathbf{x} . Stable and unstable direction in the \mathbf{x} -space in this driving system are fixed and do not dependent on \mathbf{x} . Therefore, the differential of this map is a constant matrix. In a more general situation, this is not the case, and the synchronization function must depend on both "stable" and "unstable" coordinates. Nevertheless, it is possible to understand (although it is not so simple to prove) that the dependence on the unstable coordinate is non-essential in the hyperbolic situations. The simplest way to be convinced is to remember that for hyperbolic attractor there exists a local Hölder-continuous change of variables such that in new variables the stable and unstable directions are along the coordinate lines (planes) and the situation becomes very similar to the example considered.

We examined the influence of external noise on the

function improvement. We found that noise in the data acquired from the response system sets a limit for the accuracy of the function approximation and, as the result, after some critical value of m the further increase of delay becomes useless.

To conclude we would like to emphasize that, although we apply our study to the theory of chaos synchronization, the data analysis method and theory developed here can be useful for other applications. Such applications include prediction of chaotic dynamical behavior in time and space and other studies associated with various types of prediction. The use of hybrid, "continuous-symbolic" representation of the chaotic trajectories enables one to take into account additional information about the trajectory in a compact way.

VI. ACKNOWLEDGMENTS

The authors are grateful to A. Cordonet, J. Urias, L.S. Tsimring, H.D.I. Abarbanel, and M.I. Rabinovich for stimulating discussions. This work was supported in part by a grant from the University of California Institute for Mexico and the United States (UC MEXUS) and the Consejo Nacional de Ciencia y Tecnologia de México (CONACYT). N.R. was sponsored in part by U.S. Department of Energy (grant DE-FG03-95ER14516) and the U.S. Army Research Office (MURI grant DAAG55-98-1-0269). V.A was partially supported by CONACyT grant 36445-E.

-
- [1] L. Glass and M.C. Mackey, *From clocks to chaos: the rhythms of life* (Princeton, N.J. : Princeton University Press, 1988), 248.
 - [2] N. Minorsky, *Nonlinear oscillations*, [Huntington, N.Y., R. E. Krieger Pub. Co.], 1974 [c1962], 714.
 - [3] I.I. Blekhman, *Synchronization in Science and Technology* [Amer Society of Mechanical Engineers], 1988, 255.
 - [4] A. Pikovsky, M. Rosenblum, and J. Kurths *Synchronization: A Universal Concept in Nonlinear Science* [Cambridge University Press], 2002, 500.
 - [5] E. Mosekilde, Yu. Maistrenko, and D. Postnov, *Chaotic Synchronization: Applications to Living Systems* [World Scientific Publishing Co., Inc.], 2002, 440.
 - [6] S. Boccaletti, J. Kurths, G. Osipov, D.L. Valladares, and C.S. Zhou, *Physics Reports* **366**, 1 (2002).
 - [7] V. Afraimovich, N.N. Verichev and M.I. Rabinovich, *Radiophys. Quant. Electr.* **29**, 747 (1986).
 - [8] H. Fujisaka and T. Yamada. *Prog. Theor. Phys.* **69**, 32 (1984)
 - [9] L.M. Pecora and T.L. Carroll. *Phys. Rev. Lett.* **64** (1990), 821-824.
 - [10] N.F. Rulkov, M.M. Sushchik, L.S. Tsimring, and H.D.I. Abarbanel, *Phys. Rev E* **51**, 980 (1995).
 - [11] L.M. Pecora, T.L. Carroll, and J.F. Heagy, *Phys. Rev E* **52**, 3420 (1995).
 - [12] L. Kocarev and U. Parlitz, *Phys. Rev. Lett.* **76**, 1816 (1996).
 - [13] N.F. Rulkov, V.S. Afraimovich, C.T. Lewis, J.-R. Chazottes, and A. Cordonet, *Phys. Rev E* **64**, 016217 (2001).
 - [14] A. Pikovsky, M. Zaks, M. Rosenblum, G. Osipov, and J. Kurths, *Chaos* **7**, 680 (1997)
 - [15] M.A. Zaks, E.H. Park, M.G. Rosenblum, and J Kurths, *Phys. Rev. Lett* **82**, 4228 (1999).
 - [16] B. van der Pol, *Philos. Mag.*, **3**, 65 (1927).
 - [17] A.A. Andronov and A.A Witt, *Atch. Elektrotech* **16**, 280 (1930).
 - [18] H.D.I. Abarbanel, N.F. Rulkov and M.M. Sushchik, *Phys. Rev. E* **53**, 4528 (1996).
 - [19] J. Stark, *Physica D* **10**, 163 (1997).
 - [20] B.R. Hunt, E. Ott and J.A. Yorke, *Phys Rev. E* **55**, 4029 (1997);
 - [21] K. Josić, *Phys. Rev. Lett.* **80**, 3053 (1998).
 - [22] J. Stark, *Ergod. Theory Dyn. Syst.* **19**, 155 (1999).
 - [23] V. Afraimovich, J.-R. Chazottes, and A. Cordonet, *Discrete and Continuous Dyn. Systems: Ser. B* **1**, 421 (2001).
 - [24] P. So, E. Barreto, K. Josić, E. Sander, S.J. Schiff, *Phys. Rev. E* **65** 046225 (2002).
 - [25] E. Barreto, K. Josić, C. Morales, E. Sander, and P. So, *Chaos* **13** 151 (2003).
 - [26] V. Afraimovich, A. Cordonet, and N.F. Rulkov, *Phys. Rev. E* **66** 016208 (2002).
 - [27] D. He, Z. Zheng, and L. Stone, *Phys. Rev. E* **67** 026223 (2003).